Available online at www.sciencedirect.com
SCIENCE DIRECT®
PERGAMON
Engineering Fracture Mechanics 70 (2003) 2513–2526
Engineering Fracture Mechanics
www.elsevier.com/locate/engfracmech

Channel-cracking of thin films with the extended finite element method

R. Huang [a,1], J.H. Prévost [a,*], Z.Y. Huang [b], Z. Suo [b]

[a] Department of Civil & Environmental Engineering, Princeton University, Princeton, NJ 08544, USA
[b] Department of Mechanical & Aerospace Engineering, Princeton University, Princeton, NJ 08544, USA

Received 16 September 2002; received in revised form 30 January 2003; accepted 3 February 2003

Abstract

The recently developed extended finite element method (XFEM) is applied to compute the steady-state energy release rate of channeling cracks in thin films. The method is demonstrated to be able to model arbitrary singularities by using appropriate enriching functions at selected nodes with a relatively coarse mesh. The dimensionless driving force for channeling cracks is obtained as a function of elastic mismatch, crack spacing, and the thickness ratio between the substrate and the film. The results are compared with those from several previous studies when available. Emphasis is placed on the cases with compliant substrates, for which much less information is available from previous studies. It is found that, while it is quite challenging to model the cases with very compliant substrates using regular finite element method because of the strong singularities, the present approach using XFEM is relatively simple and straightforward.

Keywords: Channeling crack; Thin film; Compliant substrate; XFEM

1. Introduction

Many applications in microelectronics (e.g., interconnects and electronic packaging) often involve integrated structures with dissimilar materials. Stresses are introduced during the processes of fabrication, reliability testing, and operation. The stress field concentrates at the junctions of dissimilar materials, at the corners, or, if there exists a crack, at the crack tip. The asymptotic analyses based on elasticity showed that the stress field is singular at these points [1–3]. Analyses with traditional finite element models (FEMs) use very fine meshes near the singular points to resolve the rapidly varying stress field [4,5]. In the cases of growing cracks, continual remeshing is required [6]. Recently, a new finite element technique has been developed to model cracks and crack growth with relatively coarse meshes and without remeshing [7–9]. The method has been named by the developers as the extended finite element method (XFEM). The

* Corresponding author. Tel.: +1-609-258-5424; fax: +1-609-258-2760.
E-mail address: prevost@princeton.edu (J.H. Prévost).
[1] Present address: Aerospace Engineering and Engineering Mechanics Department, The University of Texas at Austin, Austin, TX 78712, USA.

0013-7944/$ - see front matter © 2003 Elsevier Ltd. All rights reserved.
doi:10.1016/S0013-7944(03)00083-3

robustness of XFEM has been demonstrated by several applications [10–12]. In XFEM, the standard displacement-based finite element approximation is enriched near a crack by incorporating both the discontinuous field and the singular asymptotic crack tip field. In principle, the technique can be applied to problems with arbitrary discontinuities and singularities. Belytschko et al. [13] have demonstrated the application of XFEM to arbitrary discontinuities. This paper tends to demonstrate its application to arbitrary singularities with one example: channeling cracks in a thin elastic film bonded to an elastic substrate. The strength of singularity of this particular problem depends on the elastic mismatch between the film and the substrate. Similar approach can be used to model other singularities.

The paper is organized as follows. In Section 2, we first give an overview of XFEM and then describe the approach to model channeling cracks. Section 3 develops the numerical model, and Section 4 presents the results for channeling cracks. The accuracy of the present approach is examined by comparing the results with those available from previous studies. In addition, more complete results are presented for the effects of elastic mismatch, crack spacing, and substrate thickness on the steady-state energy release rate. Section 5 discusses the special case when the substrate material is extremely compliant in comparison with the film.

2. The extended finite element method

In this section, we first give an overview of the XFEM and then describe how to apply the method to compute the steady-state energy release rate of channeling cracks in thin films.

2.1. An overview of extended finite element method

To model a crack, the regular finite element method would have to exactly mesh the geometry of the crack and use a very fine mesh near the crack tip to capture the singular stress field. When the crack grows, cumbersome remeshing is required. Several new finite element techniques have been developed to relieve the task in modeling cracks [14,15]. One recent development is to use an enrichment technique in the standard finite element framework through a partition of unity method [7–9]. The method has been named by the developers as the XFEM. An XFEM model consists of a regular FEM, which is independent of the crack geometry, and a crack representation, which is independent of the elements. Fig. 1 illustrates a typical mesh with a curved crack of two tips. The crack is represented by a piecewise linear curve. Selected nodes around the crack have extra degrees of freedom associated with the enriching functions. For the nodes around the crack tips (the circled nodes in Fig. 1), the enriching functions are derived from the near-tip asymptotic field to incorporate the stress singularity. For other nodes around the crack (the squared nodes in Fig. 1), the discontinuous Heaviside function is the only enriching function in order to incorporate the displacement jump across the crack faces. With such enrichments, the finite element discretization of the displacement field takes the form

$$\mathbf{u}(\mathbf{x}) = \sum_{i\in I} \mathbf{u}_i \phi_i(\mathbf{x}) + \sum_{j\in J} \mathbf{b}_j \phi_j(\mathbf{x}) H(\mathbf{x}) + \sum_{k\in K} \phi_k(\mathbf{x}) \left(\sum_l \mathbf{c}_{kl} F_l(\mathbf{x}) \right), \tag{2.1}$$

where K is the set of circled nodes, J is the set of squared nodes, and I is the set of all nodes. The first term at the right-hand side of Eq. (2.1) is the regular finite element approximation with $\mathbf{u}_i$ as the nodal displacements, and the other two terms are enrichments with extra degrees of freedom, $\mathbf{b}_j$ and $\mathbf{c}_{kl}$, for the nodes in sets J and K, respectively. $\phi_i(\mathbf{x})$ are the standard finite element shape functions. $H(\mathbf{x})$ is the Heaviside "jump" function which is defined in the local coordinate system so that it equals to 1 at one side of the

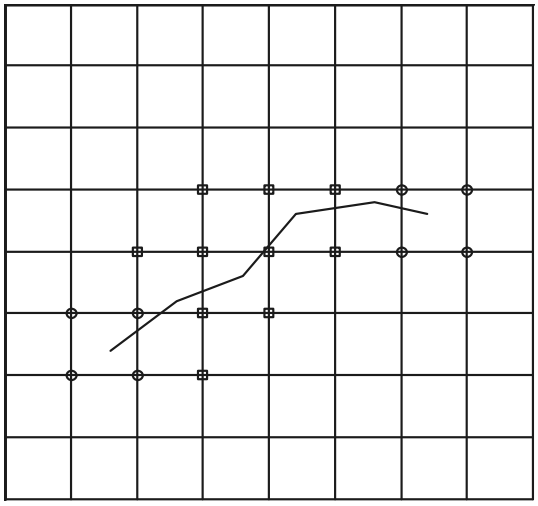

Fig. 1. A typical XFEM mesh with a curved crack of two tips. The squared nodes are enriched with the Heaviside function, and the circled nodes are enriched with the near-tip asymptotic field.

crack and equals to -1 at the other side. $F_l(\mathbf{x})$ are the functions that span the asymptotic displacement field at the crack tip. For two-dimensional elasticity problems, the functions $F_l(\mathbf{x})$ are

$$\{F_l(\mathbf{x}), l = 1, \ldots, 4\} = \left\{\sqrt{r}\sin\left(\frac{\theta}{2}\right), \sqrt{r}\cos\left(\frac{\theta}{2}\right), \sqrt{r}\sin\left(\frac{\theta}{2}\right)\sin(\theta), \sqrt{r}\cos\left(\frac{\theta}{2}\right)\sin(\theta)\right\}, \tag{2.2}$$

where (r, θ) are the local polar coordinates at the crack tip.

In the discretization of Eq. (2.1), the displacement field is global, but the supports of the enriching functions are local because they are multiplied by the nodal shape functions. With such discretization and enrichment, the finite element mesh can be considerably coarse near the crack tip, as the singularity has been taken into account by the enriching functions. Furthermore, the elements need not to conform to the crack geometry, which makes mesh generation very convenient, especially for curved cracks. Another great advantage of this method is for growing cracks. No remeshing is necessary! As the crack grows, one only needs to update the sets of nodes that are to be enriched, while the mesh remains unchanged.

The robustness of XFEM has been demonstrated by several applications [10–12], for both stationary and slow growing cracks. It has also been applied to three-dimensional cracks [16] and arbitrary discontinuities such as voids and inclusions [13]. In this paper, we demonstrate another application of XFEM aiming for problems with different singularities. When modeling integrated structures with dissimilar materials, stress singularities are ubiquitously present at locations such as material junctions, corners, and crack tips. The strength of each singularity depends on the properties of the surrounding materials. Modeling such structures with the traditional finite element method is tedious since a very fine mesh has to be generated around each singular point [4,5]. On the other hand, a simpler mesh may be used in an XFEM model with appropriate enriching functions. The enriching functions (2.2) were derived from the asymptotic field at the crack tip in a two-dimensional homogeneous elastic body. Similar asymptotic fields are available for other singularities [1–3]. For a different singularity, a different set of enriching functions can be derived from the corresponding asymptotic field. In principle, the XFEM technique can be applied to arbitrary singularities. As an example of such applications, the remainder of this paper will focus on channeling cracks in thin films, where the strength of the singularity depends on the elastic mismatch between the film and the substrate.

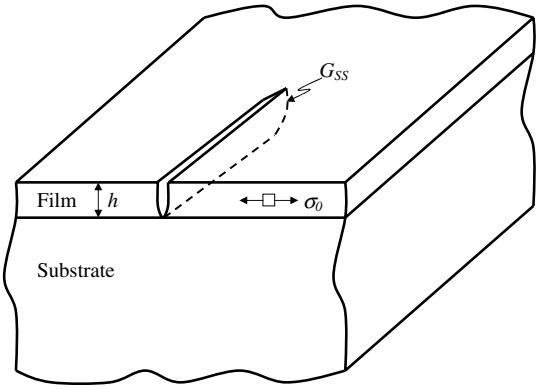

Fig. 2. A crack channeling through a pre-tensioned film on a semi-infinite substrate.

2.2. Extended finite element method for channeling cracks

Fig. 2 shows a crack channeling through a pre-tensioned film on a semi-infinite substrate. The crack is arrested by the film/substrate interface in the direction perpendicular to the interface but advances in the direction parallel to the interface. The crack front takes a curved shape so that the energy release rate at every point of the front is the same. The problem is three-dimensional (3D) in nature. After the crack length exceeds a few times the film thickness, the crack asymptotically approaches a steady state: the entire front maintains its shape as the crack advances, and so does the opening profile in the wake. A 3D analysis of crack channeling in an elastic film bonded to a rigid substrate indicated that the steady state is achieved for crack lengths two to three times the film thickness [17]. Recently, Ambrico and Begley [18] showed that the crack length to achieve the steady state is significantly larger when the substrate is more compliant than the film. Here we will only consider cracks channeling at the steady state, in which case the energy release rate at the channel front can be evaluated using two plane-strain problems, that is, by subtracting the strain energy stored in a unit slice far behind of the front from that far ahead [19]. Both problems can be solved with no knowledge about the shape of the channel front. The stress state far ahead of the channel front is trivial: the film is subject to a uniform residual stress σ_0 and the substrate is stress-free (Fig. 3a). The stress state at the wake far behind of the front is identical to that in a film with a plane-strain through-crack (Fig. 3b). Let $\delta(z)$ be the opening displacement of the plane-strain crack. By the energy argument, the energy release rate at the channel front is

$$G_{\mathrm{ss}} = \frac{\sigma_0}{2h}\int_0^h \delta(z)\,\mathrm{d}z. \tag{2.3}$$

Thus, to compute the steady-state energy release rate, one only needs to solve the plane-strain problem in Fig. 3b for the opening displacement, $\delta(z)$.

The singularity at the crack tip of the plane-strain problem in Fig. 3b depends on the elastic mismatch between the film and the substrate. Dundurs [20] introduced two parameters to characterize the elastic mismatch

$$\alpha = \frac{\mu_1(\kappa_2+1)-\mu_2(\kappa_1+1)}{\mu_1(\kappa_2+1)+\mu_2(\kappa_1+1)}, \tag{2.4}$$

$$\beta = \frac{\mu_1(\kappa_2-1)-\mu_2(\kappa_1-1)}{\mu_1(\kappa_2+1)+\mu_2(\kappa_1+1)}, \tag{2.5}$$

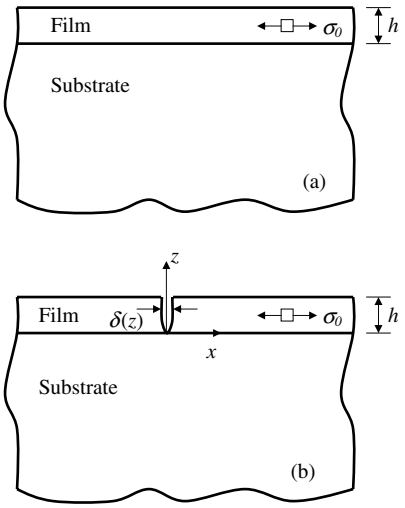

Fig. 3. Schematics of the two plane-strain problems for a steady-state channeling crack, with (a) and (b) for far ahead of the channel front and far behind of the channel front, respectively.

where μ_j is the shear modulus of material j with $j = 1$ for the film and $j = 2$ for the substrate, v_j is Poisson's ratio, and $\kappa_j = 3 - 4v_j$ under the plane-strain condition. The stress just ahead of the crack tip is of the form

$$\sigma_{xx}(0,z) = C\frac{\sigma_0 h^s}{(-z)^s}, \tag{2.6}$$

where C is a dimensionless number. The stress singularity exponent, s, is a function of Dundurs parameters and is the root to the transcendental equation derived by Zak and Williams [2]

$$\cos(s\pi) - 2\frac{\alpha-\beta}{1-\beta}(1-s)^2 + \frac{\alpha-\beta^2}{1-\beta^2} = 0. \tag{2.7}$$

The value of s as a function of α and β was plotted in [19] and listed in a table by Beuth [21]. In the case of no elastic mismatch ($\alpha = \beta = 0$), the stress singularity reduces to the square root singularity of a crack tip in a homogeneous elastic material, i.e., $s = 0.5$. When the substrate is stiffer than the film ($\alpha < 0$), the singularity is weaker, i.e., $s < 0.5$. When the substrate is more compliant than the film ($\alpha > 0$), the singularity is stronger, i.e., $s > 0.5$. For an extremely compliant substrate ($\alpha \to 1$), the singularity exponent approaches 1 ($s \to 1$).

The asymptotic displacement field near the tip of the plane-strain through-crack takes the form

$$\mathbf{u}_j(r,\theta) = r^{1-s}\{\mathbf{a}_j\cos(s\theta) + \mathbf{b}_j\sin(s\theta) + \mathbf{c}_j\cos[(s-2)\theta] + \mathbf{d}_j\sin[(s-2)\theta]\}, \tag{2.8}$$

where $\mathbf{a}_j$, $\mathbf{b}_j$, $\mathbf{c}_j$, $\mathbf{d}_j$ are constant vectors for the corresponding material (again, $j = 1$ for the film and $j = 2$ for the substrate), and (r,θ) are the local polar coordinates with the origin at the crack tip. The asymptotic displacement field, Eq. (2.8), is contained in the span of the following four functions:

$$\{F_l^*(r,\theta), l = 1,\ldots,4\} = \left\{r^{1-s}\cos(s\theta), r^{1-s}\sin(s\theta), r^{1-s}\cos[(s-2)\theta], r^{1-s}\sin[(s-2)\theta]\right\}. \tag{2.9}$$

By replacing the enriching functions F_l (Eq. (2.2)) with the functions F_l^* in the displacement discretization (2.1), the XFEM technique can be used to solve the plane-strain problem of Fig. 3b with arbitrary elastic mismatch between the film and the substrate. The solution for the opening displacement along the crack, $\delta(z)$, is then integrated to compute the steady-state energy release rate of the channeling crack (Eq. (2.3)).

3. Numerical model

Fig. 4a shows the geometry and the boundary conditions of the plane-strain problem. The crack is represented by the line EF. The thickness of the film is h. The substrate also has a finite thickness H and is simply supported at B and C. Along the vertical boundaries AB and CD, the roller boundary condition is assumed, through which we are actually modeling a periodic set of parallel cracks of spacing S. Other boundaries are traction free. The film is subjected to an initial tensile stress σ_0. At equilibrium, the film and the substrate deform so that the tractions along the crack faces vanish and the crack opens. For each set of material properties of the film and the substrate, solutions were sought with various values of S/h and H/h in order to obtain the asymptotic solution for an isolated single crack ($S/h \to \infty$) with a semi-infinite substrate ($H/h \to \infty$) and to investigate the effects of crack spacing and substrate thickness.

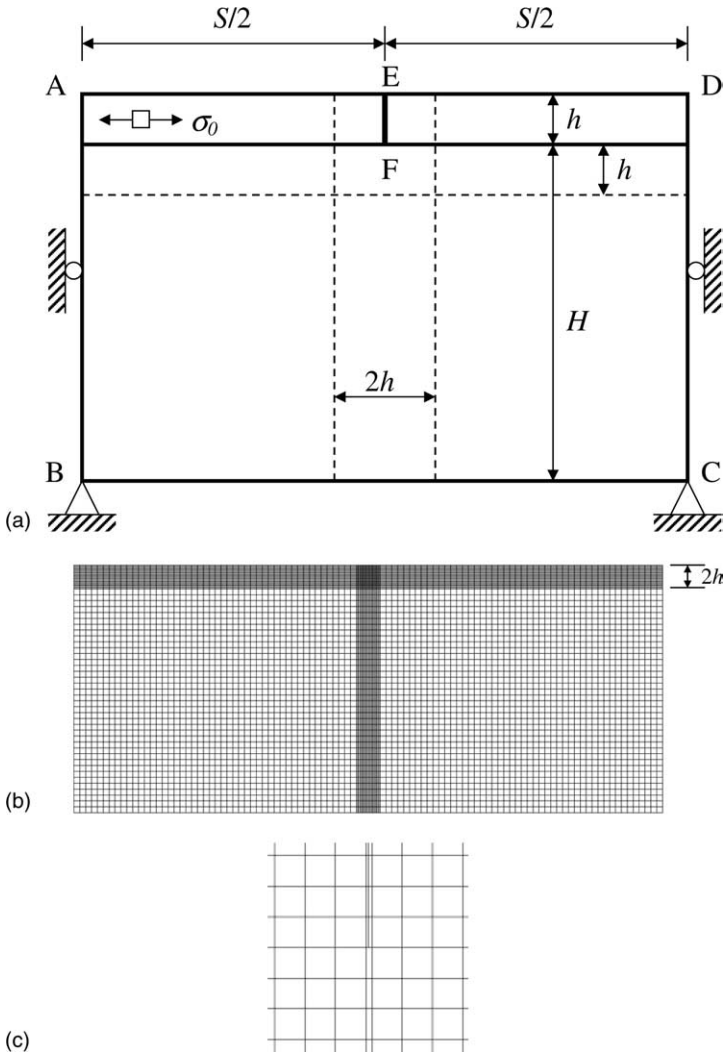

Fig. 4. The XFEM model of the plane-strain problem: (a) geometry and boundary conditions; (b) a example mesh; (c) a detailed mesh around the crack tip.

Table 1
Results of the convergence study for the case with no elastic mismatch between the film and the substrate ($\alpha = \beta = 0$, $H/h = 20$, $S/h = 50$)

N	5	10	20	30
Error (%)	5.3	2.1	0.8	0.5

N is the number of elements across the film thickness in the XFEM model, and the errors are computed relative to Eq. (3.1).

The finite element meshes are generated as follows. First divide the whole domain into six regions, as indicated by the dashed lines in Fig. 4a. In each of the six regions, a uniform mesh is generated with the first-order four-node quadrilateral elements. In the upper-central region, the one with the crack, the mesh is relatively fine. In the lower-left and lower-right regions, the mesh is coarse. In the other three regions, the mesh is generated such that it is compatible with the adjacent regions. Fig. 4b shows an example of the resulting mesh, and Fig. 4c shows the detail around the crack tip. In the following analyses, the mesh is characterized by the mesh density in the upper-central region, because the mesh around the crack is the most important for the accuracy of the results. Let N be the number of elements across the film thickness. The upper-central region consists of $2N \times 2N + 1$ elements, where one more element is used in the lateral direction so that the crack aligns along the center of the elements as shown in Fig. 4c. Such alignment of the crack with the elements is not necessary for XFEM, but is convenient for the computation of the opening displacement. The meshes in the other regions are less important and they are generated accordingly with reasonable aspect ratios.

Convergence studies were conducted to determine the appropriate mesh density. For a film/substrate combination with no elastic mismatch, the steady-state energy release rate G_{ss} can be obtained from the solution for an edge crack in a homogeneous half-plane [22], as given in [19]

$$G_{ss} = 1.976\frac{\sigma_0^2 h}{E^*}, \tag{3.1}$$

where $E^* = E/(1 - \nu^2)$ is the plane-strain modulus of the film and the substrate. The results from the XFEM model with different mesh densities are compared to (3.1) and the errors are listed in Table 1. The mesh density is characterized by N, the number of elements across the film thickness. The error decreases as N increases and is less than 1% when $N = 20$. No significant improvement was achieved with $N > 20$. Further convergence studies for film/substrate combinations with elastic mismatches showed that $N = 20$ is generally sufficient for accuracy of about 1%.

4. Results and discussions

In the previous studies of cracking in thin films (e.g., [19]), a unifying dimensionless number Z has been defined such that the energy release rate for a crack is

$$G_{ss} = Z\frac{\sigma_0^2 h}{E_1^*}, \tag{4.1}$$

where E_1^* is the plane-strain modulus of the film. The number Z is a dimensionless driving force, depending on the cracking pattern. The practical significance of this dimensionless number was first documented by Evans et al. [23]. For the channeling crack in the present study, the number Z depends on the Dundurs parameters α and β, the thickness ratio H/h, and the dimensionless crack spacing S/h. Beuth [21] carried out an analysis for a single channeling crack ($S/h \to \infty$) in a thin film on a semi-infinite substrate ($H/h \to \infty$) with various elastic mismatches. Specifically, for the case with no elastic mismatch ($\alpha = \beta = 0$), Eq. (3.1) leads to $Z = 1.976$. The effect of crack spacing was discussed in [19] and [24], but limited to the

case with no elastic mismatch. Recently, Xia and Hutchinson [25] proposed a two-dimensional model for crack patterns in thin films and obtained a semi-analytical formula for the steady-state energy release rate of parallel cracks with the effects of elastic mismatch and crack spacing. In the present study, we compute the opening displacement $\delta(z)$ using the XFEM model constructed in the previous section, and then in-

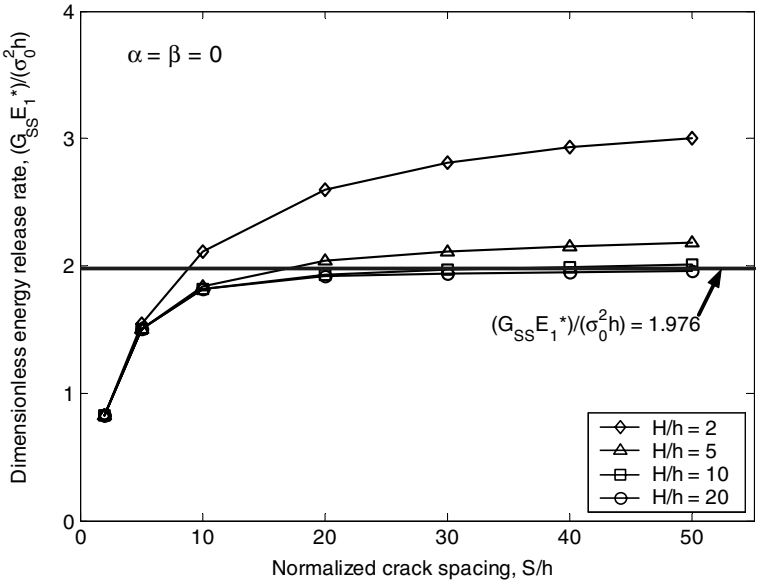

Fig. 5. The dimensionless energy release rate of channeling cracks for zero elastic mismatch between the film and the substrate.

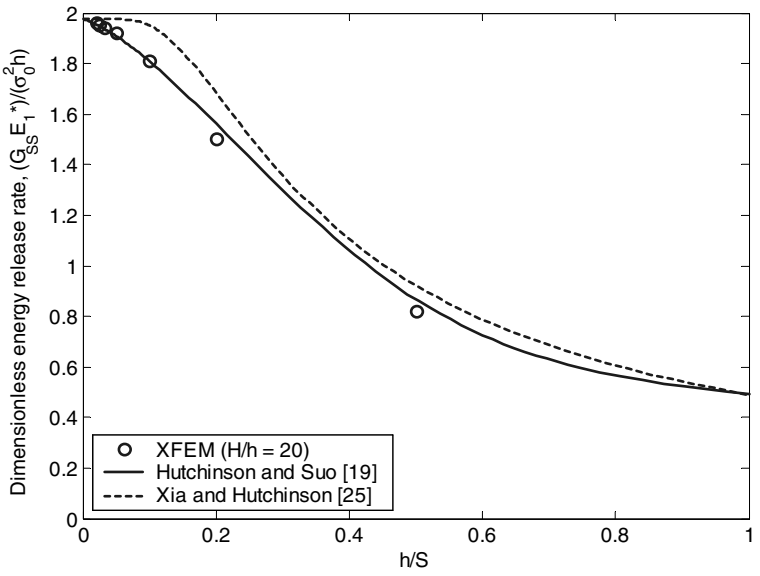

Fig. 6. The effect of crack spacing on the energy release rate of parallel channeling cracks with a semi-infinite substrate and no elastic mismatch.

tegrate it to obtain the energy release rate (Eq. (2.3)). The results are compared to those from the previous studies when available. In addition, the effect of finite substrate thickness is included so that the condition under which the substrate can be approximated as semi-infinite is clear.

Fig. 5 shows the results for the case with no elastic mismatch between the film and the substrate. The dimensionless energy release rate is plotted as a function of the normalized crack spacing S/h for various thickness ratios, H/h. A thinner substrate is more compliant and the corresponding energy release rate is larger. The results become indistinguishable for $H/h \geqslant 20$. In other words, the results saturate into one curve for thickness ratios larger than 20. Thus, in the case of no elastic mismatch, $H/h = 20$ is sufficient for a substrate to be considered semi-infinite. For a given thickness ratio, the energy release rate increases as the crack spacing increases and asymptotically approaches the energy release rate for a single channeling crack. For the case $H/h = 20$, the value of Z approaches 1.976. The computed value of Z for $H/h = 20$ and $S/h = 50$ is 1.960; the difference is less than 1%.

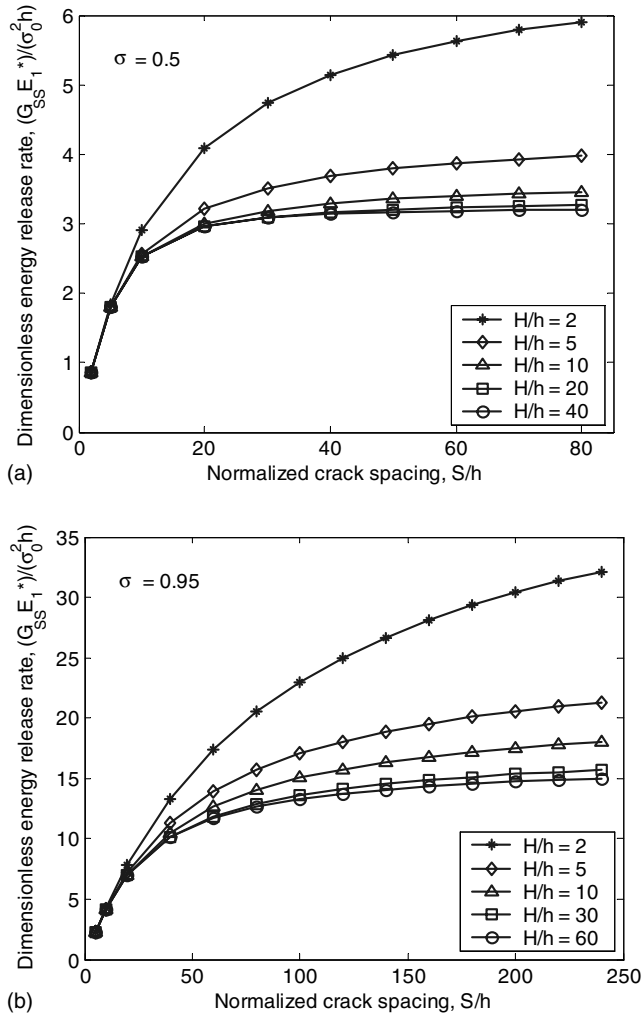

Fig. 7. The dimensionless energy release rate of channeling cracks for two different elastic mismatches between the film and the substrate: (a) $\alpha = 0.5$ and (b) $\alpha = 0.95$ ($\beta = \alpha/4$ in both cases).

For the special case with no elastic mismatch and with a semi-infinite substrate, the energy release rate of parallel cracks can be obtained with a high accuracy using the solution in [22] for parallel edge cracks in a semi-infinite plane. The result was plotted as a function of h/S in [19] and is reproduced as the solid curve in Fig. 6. The circles in Fig. 6 are the computed results from the present study for $H/h = 20$. The dashed curve is the semi-analytical solution by Xia and Hutchinson [25] using an approximate model. Evidently, the present numerical solutions agree with the solid curve closely, but the dashed curve overestimates the energy release rate by a few percents.

Fig. 7 shows the results for the cases with two different elastic mismatches between the film and the substrate. In both cases, the substrate is more compliant than the film. For the cases with a substrate stiffer than the film, the results are similar to that with no elastic mismatch (Fig. 5). In all calculations, the Poisson's ratio is set to be 1/3 for both the film and the substrate, so that the two Dundurs parameters become $\alpha = (E_1 - E_2)/(E_1 + E_2)$ and $\beta = \alpha/4$. Previous studies have shown that the energy release rate depends on β weakly. In each plot of Fig. 7, as the thickness ratio increases, the curves converge to a curve for the case with a semi-infinite substrate ($H/h \to \infty$); the convergence is slower when the substrate material is more compliant. To approximate a semi-infinite substrate, we use a sufficiently large thickness ratio, which is 20 for $\alpha = 0$ (see Fig. 5), 40 for $\alpha = 0.5$, and 60 for $\alpha = 0.95$. For a fixed thickness ratio, the energy release rate increases as the crack spacing increases and asymptotically approaches a value that corresponds to the case with an isolated single crack (i.e., $S/h \to \infty$); the approaching is also slower when the substrate material is more compliant.

Beuth [21] computed the energy release rate of a single channeling crack for a semi-infinite substrate with various elastic mismatches using a dislocation formulation and solution procedure. To compare with his results, we use a sufficiently large thickness ratio and a sufficiently large spacing to approximate a single crack with a semi-infinite substrate. Both the thickness ratio and the spacing for such approximation depend on the elastic mismatch; larger thickness ratio and larger spacing are used when the substrate material is more compliant, as advised by Fig. 7. Fig. 8 shows the comparison between the present study and

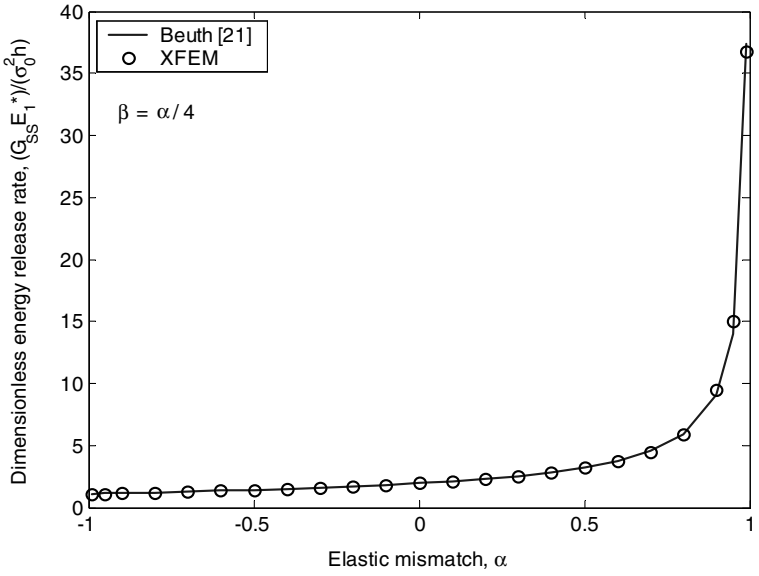

Fig. 8. The dimensionless energy release rate of a single channeling crack in a thin film bonded to a semi-infinite substrate as a function of the elastic mismatch.

Beuth [21]. The difference between the two is less than 1%, except for the three largest elastic mismatches with $\alpha \geqslant 0.9$. We discuss these cases in Section 5.

5. On very compliant substrates

The driving force for channeling cracks becomes extremely large when the substrate material is very compliant. For a single crack on a semi-infinite substrate, the results from the present numerical model differ from those in Beuth [21] by a few percents when the Dundurs parameter α is greater than 0.9, as listed in Table 2. The computed values of Z from the XFEM model are greater than Beuth's values for $\alpha = 0.9$ and 0.95, but is less than Beuth's value for $\alpha = 0.99$. We noticed that very large crack spacing and thickness ratio have to be used in the case $\alpha = 0.99$ to obtain the asymptotic result for a single crack with a semi-infinite substrate. The value in Table 2 for $\alpha = 0.99$ is obtained by using $S/h = 800$ and $H/h = 100$. However, as shown in Fig. 9, the result has not reached the asymptote yet, and using a larger spacing, S/h, would yield a larger value of Z. The asymptotic result for $\alpha = 0.99$ is expected to be greater than Beuth's result as it is for $\alpha = 0.9$ and 0.95. However, due to the computational limit, we were not able to reach the asymptotic solution for $\alpha = 0.99$.

Table 2
Comparisons of the results from Beuth [21], the XFEM model, and the regular FEM models with two different crack-tip element sizes for the dimensionless driving force of a single channeling crack in a thin film bonded to a semi-infinite and very compliant substrate

α	0.9	0.95	0.99
Z (Beuth [21])	9.071	14.04	37.43
Z (XFEM)	9.475	14.99	36.79
Z (regular FEM, $h/h^c = 10^3$)	8.783	12.92	23.86
Z (regular FEM, $h/h^c = 10^7$)	9.124	13.88	30.45

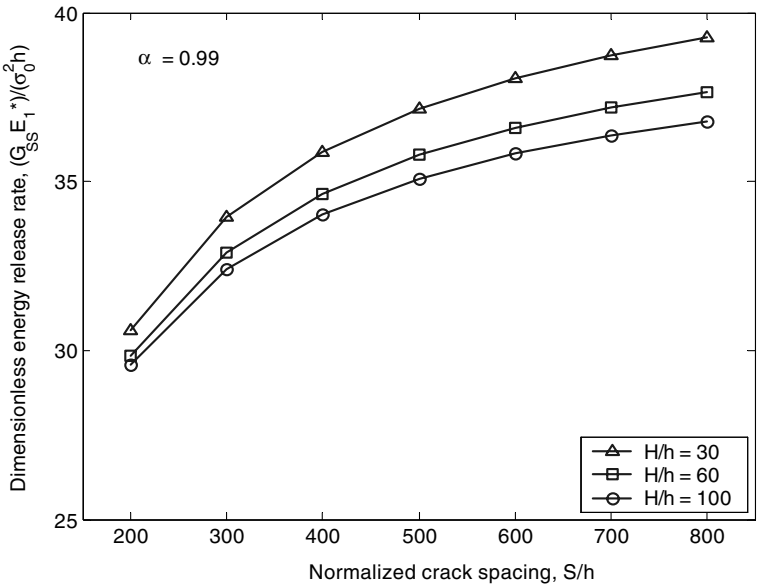

Fig. 9. The dimensionless energy release rate of channeling cracks for the elastic mismatch $\alpha = 0.99$.

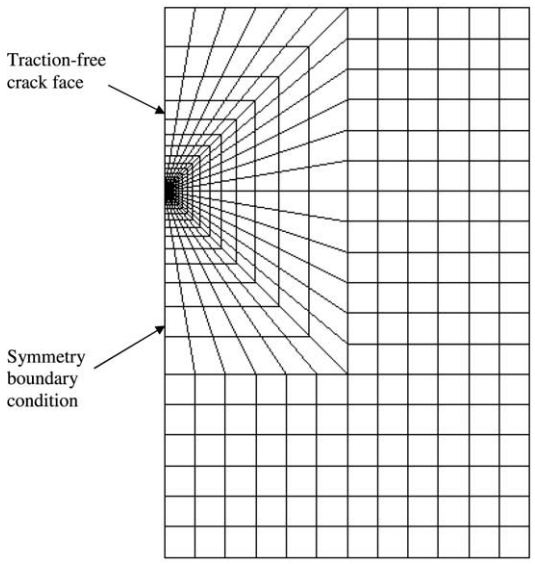

Fig. 10. A typical mesh near the crack for the regular FEM.

The same problem can be solved using a regular FEM with a very fine mesh near the crack tip. Fig. 10 shows a typical mesh near the crack generated by ABAQUS. The second-order eight-node quadrilateral elements were used together with a set of six-node triangular elements around the crack tip. Let h^e be the size of the elements near the crack tip. By using an element size near the crack tip of about three orders of magnitude smaller than the film thickness, i.e., $h/h^e = 10^3$, we were able to compute the energy release rate with the accuracy of about 1% for $\alpha < 0.9$. For $\alpha \geqslant 0.9$, however, the results differ from those in both Beuth [21] and the present study using the XFEM model, and an even finer mesh has to be used. Table 2 lists the computed energy release rates for a single crack on a semi-infinite substrate approximated by using the spacing $S/h = 400$ and the thickness ratio $H/h = 100$. Two different crack tip element sizes were used. With the crack-tip element size reduced down to seven orders of magnitude smaller than the film thickness (i.e., $h/h^e = 10^7$), the results compare better with those from Beuth and the XFEM model. Again, $S/h = 400$ is not large enough to compute the asymptotic value for $\alpha = 0.99$. To further illustrate the requirement for very fine mesh in the regular FEM models, Table 3 lists the results from both the XFEM model and the regular FEMs for a small sample with $S/h = 4$ and $H/h = 2$. For the elastic mismatch $\alpha = 0$, the result from the regular FEMs converges when the mesh density near the crack tip is two orders of magnitude smaller than the film thickness, and the result is within 1% comparing to that from the XFEM model. For

Table 3
Comparisons of the computed results from the XFEM model and the regular FEM models with various element sizes near the crack tip

Model	h/h^e	Z ($\alpha = 0$)	Z ($\alpha = 0.99$)
XFEM	20	1.363	1.926
Regular FEM	10^2	1.373	1.779
Regular FEM	10^3	1.374	1.819
Regular FEM	10^4	–	1.846
Regular FEM	10^5	–	1.863
Regular FEM	10^6	–	1.874
Regular FEM	10^7	–	1.882

the elastic mismatch $\alpha = 0.99$, however, the result from the regular FEMs converges very slowly and differs from the result of the XFEM model by about 2% when the mesh density near the crack tip is down to seven orders of magnitude smaller than the film thickness. Larger difference is expected when S/h and H/h are larger. Such requirement for a finer mesh with a larger α is due to the fact that the stress singularity at the crack tip increases with the elastic mismatch. As we discussed in Section 3, the stress singularity exponent s is 0.5 for $\alpha = 0.5$ and is about 0.94 for $\alpha = 0.99$. In contrast to the requirement of a finer mesh for a stronger singularity in the regular FEM models, the XFEM model resolves the stress singularity by nodal enrichments and the same mesh can be used for different singularities.

6. Conclusions

We apply the XFEM to compute the steady-state energy release rate of channeling cracks in thin films. The singularity of the deduced plane-strain problem depends on the elastic mismatch between the film and the substrate. The result demonstrates that the XFEM techniques can be applied to model problems with the singularity exponent ranging from below 0.5 to nearly 1. In principle the method can be applied to arbitrary singularities.

The dimensionless driving force for channeling cracks is obtained as a function of elastic mismatch, crack spacing, and thickness ratio between the substrate and the film, from which the asymptotic result for the case with a single crack and a semi-infinite substrate is extracted. Comparisons with the available previous studies show good general agreements. The relatively large differences for cases when the substrate is much more compliant than the film is discussed. Regular FEMs are used to support our discussions and to show the advantages of the XFEM method.

Acknowledgements

The work is supported by the National Science Foundation through grants CMS-9820713 and CMS-9988788 with Drs. Ken Chong and Jorn Larsen-Basse as the program directors, and by the New Jersey Science and Technology Commission.

References

[1] Williams ML. Stress singularities resulting from various boundary conditions in angular corners of plates in extension. J Appl Mech 1952;19:526–8.
[2] Zak AR, Williams ML. Crack point stress singularities at a bi-material interface. J Appl Mech 1963;30:142–3.
[3] Bogy DB. 2 edge-bonded elastic wedges of different materials and wedge angles under surface tractions. J Appl Mech 1971;38:377.
[4] Liu XH, Suo Z, Ma Q. Split singularities: stress field near the edge of a silicon die on a polymer substrate. Acta Mater 1999;47:67–76.
[5] Ambrico JM, Jones EE, Begley MR. Cracking in thin multi-layers with finite-width and periodic architectures. Int J Solids Struct 2002;39:1443–62.
[6] Swenson D, Ingraffea A. Modeling mixed-mode dynamic crack propagation using finite elements: theory and applications. Comput Mech 1988;3:381–97.
[7] Belytschko T, Black T. Elastic crack growth in finite elements with minimal remeshing. Int J Numer Meth Engng 1999;45:601–20.
[8] Moës N, Dolbow J, Belytschko T. A finite element method for crack growth without remeshing. Int J Numer Meth Engng 1999;46:131–50.
[9] Moës N, Belytschko T. Extended finite element method for cohesive crack growth. Engng Fract Mech 2002;69:813–33.
[10] Sukumar N, Srolovitz DJ, Baker TJ, Prevost JH. Brittle fracture in polycrystalline microstructures with the extended finite element method. Int J Numer Meth Engng 2003;56:2015–37.

[11] Huang R, Prevost JH, Suo Z. Loss of constraint on fracture in thin film structures due to creep. Acta Mater 2002;50:4137–48.
[12] Liang J, Huang R, Prevost JH, Suo Z. Thin film cracking modulated by underlayer creep. Exp. Mech., in press.
[13] Belytschko T, Moës N, Usui S, Parimi C. Arbitrary discontinuities in finite elements. Int J Numer Meth Engng 2001;50:993–1013.
[14] Oliver J. Continuum modeling of strong discontinuities in solid mechanics using damage models. Comput Mech 1995;17:49–61.
[15] Rashid MM. The arbitrary local mesh refinement method: an alternative to remeshing for crack propagation analysis. Comput Meth Appl Mech Engng 1998;154:133–50.
[16] Sukumar N, Moës N, Moran B, Belytschko T. Extended finite element method for three-dimensional crack modeling. Int J Numer Meth Engng 2000;48:1549–70.
[17] Nakamura T, Kamath SM. Three-dimensional effects in thin-film fracture mechanics. Mech Mater 1992;13:67–77.
[18] Ambrico JM, Begley MR. The role of initial flaw size, elastic compliance and plasticity in channel cracking of thin films. Thin Solid Films 2002;419:144–53.
[19] Hutchinson JW, Suo Z. Mixed mode cracking in layered materials. Adv Appl Mech 1992;29:63–191.
[20] Dundurs J. Edge-bonded dissimilar orthogonal elastic wedges. J Appl Mech 1969;36:650–2.
[21] Beuth JL. Cracking of thin bonded films in residual tension. Int J Solids Struct 1992;29:1657–75.
[22] Tada H, Paris PC, Irwin GR. The stress analysis of cracks handbook. 3rd ed. New York: ASME Press; 2000.
[23] Evans AG, Drory MD, Hu MS. The cracking and decohesion of thin films. J Mater Res 1988;3:1043–9.
[24] Thouless MD. Crack spacing in brittle films on elastic substrates. J Am Ceram Soc 1990;73:2144–6.
[25] Xia ZC, Hutchinson JW. Crack patterns in thin films. J Mech Phys Solids 2000;48:1107–31.